Granular Matter (2010) 12:303–316
DOI 10.1007/s10035-010-0182-y

# A laboratory investigation on an undisturbed silty sand from a slope prone to landsliding

**Francesca Casini · Cristina Jommi · Sarah Springman**

Received: 20 May 2009 / Published online: 26 March 2010


**Abstract** A laboratory investigation is presented for undisturbed samples of a silty sand under saturated conditions. The soil was sampled from test pits south of Rüdlingen in North–East Switzerland, where a landslide triggering experiment was carried out on a steep forest slope. The aim of the work was to characterise the behaviour of the soil in triaxial tests, in the light of the possible failure mechanisms of the slope. Conventional drained and undrained triaxial tests were conducted to detect critical state conditions as well as peak shear strength as a function of confining pressure. Soil specimens were also exposed to stress paths simulating in situ water pressure increase to study the stress–strain response and to enhance the ability to predict failure conditions more accurately in the future. Possible unstable response along the stress paths analysed was investigated by means of second order work and strain acceleration. The results show that temporary unstable conditions may be encountered for this soil at stress ratios below ultimate failure and even below critical state line, depending on void ratio, drainage conditions and time dependent compressibility. A modified state parameter is explored as a potentially useful tool to discriminate conditions leading to eventual collapse.

**Keywords** Laboratory tests · Undisturbed silty sand · Instability · Slope analysis

F. Casini (✉) · S. Springman
ETH Zürich, Wolfgang Pauli-Strasse 15, 8093 Zürich, Switzerland
e-mail: francesca.casini@igt.baug.ethz.ch

C. Jommi
Politecnico di Milano, piazza Leonardo da Vinci 32, 20133 Milano, Italy

## 1 Introduction

This investigation was conducted within the context of a multi-disciplinary research project about triggering of rapid mass movements in steep terrain, called TRAMM. The primary focus of this research project is to enhance the understanding of triggering and initiation mechanisms, including the transition from slow to fast mass movement processes, and flow characteristics of such catastrophic mass movements (http://www.cces.ethz.ch/projects/hazri/tramm). The influence of rainfall events on slope stability is studied in a sub-project, by instrumenting a natural slope in Rüdlingen, Switzerland, and subjecting it to a series of artificial rainfall events. The project was designed to replicate the effects of a heavy rainfall event in May 2002, in which 100 mm rain fell in 40 min [1], causing 42 surficial landslides.

To understand the hydro-mechanical conditions leading to initiation of failure mechanisms better, an extensive soil investigation was conducted to understand how the strength is mobilised in the soil and how this may be related to change in water content and void ratio in the slope. The investigation started from the analysis of the behaviour of the undisturbed soil in saturated conditions, which is presented and discussed herein.

## 2 Landslide test site

The experimental area is located on an east facing slope on the banks of the river Rhine (Fig. 1a). The altitude is about 350 m above sea level. The average gradient was determined using a total station theodolite to be 38° with maximum of 43° in the middle of the slope. The surface is slightly concave; the middle longitudinal line is 0.3–0.5 m lower than the sides, except that the slope drains marginally to the north at the

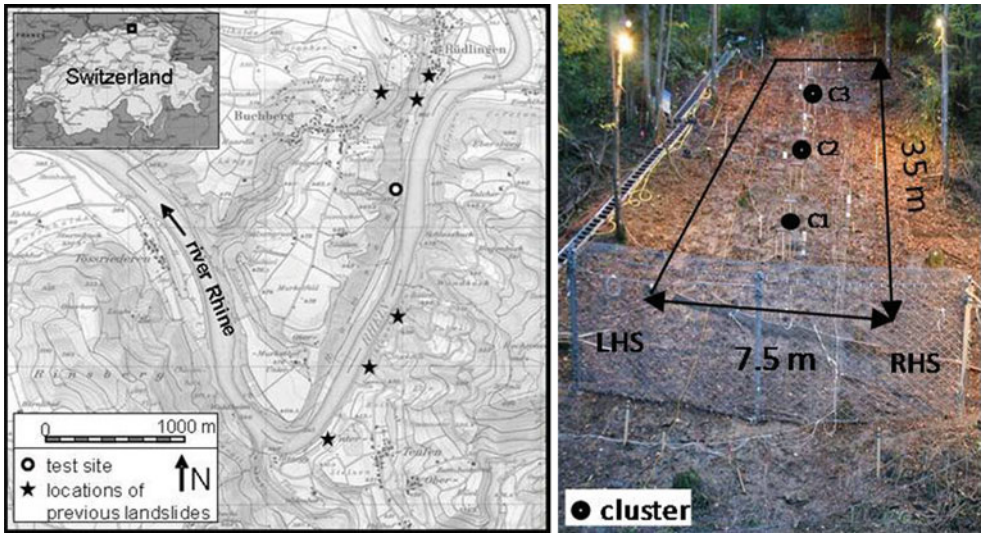


**Fig. 1** Location of the site: **a** detailed map; **b** test site, geometry and 3 instrument clusters (C1–C3)

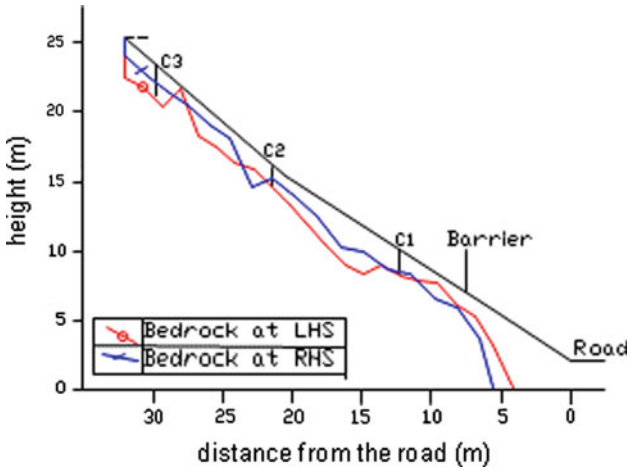


**Fig. 2** Cross section through the slope on the *left hand* (LHS) and *right hand* (RHS), reference to Fig. 1b

bottom [2]. According to DPL tests (Dynamic Probing with a "Light" 10 kg weight), the bedrock level is reached between 0.5 and 5 m (Fig. 2). The site is located in the Swiss lowlands and the underlying rock consists mainly of a sequence of Molasse, which is the naturally cemented sediment that was deposited in the foreland basin of the Alps under successive fresh and saltwater regimes.

Three cluster locations (Figs. 1b, 2) were instrumented with tensiometers, Decagons, TDRs, piezometers, rain gauges, pressure cells, and deformation probes. The instruments were installed from 15 to 150 cm depth below the surface at each of three cluster locations.

Combined sprinkling and dye tracer tests were carried out at the three different locations, revealing a high infiltration capacity of the soil. No overland flow was observed during the sprinkling at any of the locations. In all of the soil profiles, staining of the soil was mainly homogeneous and little preferential flow was visible, although deeper percolation into the Molasse sandstone was revealed by the observation of several stained joints below the subsoil.

The slope was subjected to extreme rainfall through artificial means in October 2008 over a period of 4 days, with a rainfall intensity of 15 mm/h for two days and an intensity of 30 mm/h for the last two days. The sprinklers were distributed at constant spacing along the central line of the slope. Some surface movements were detected during this extreme event, although failure did not occur. Subsequently, a range of measures were implemented, such as relocating the distribution of the sprinklers to provide more rainfall to the upper part of the slope, so that a failure mechanism was triggered in March 2009, incorporating about 150 $m^3$ of debris.

## 3 Classification of the soil

Soil was collected from test pits (TPs) at different depths. The grain size distribution, the natural water content, together with consistency limits and activity, are shown with depth for the time of sampling for TP1 in Fig. 3. The mean physical properties of interest in the current experimental programme are summarised in Table 1. The data for TP1 may be considered representative of the whole test site.

The top soil is a loose silty sand with significant macroporosity around grain accumulations or peds. It can be classified as medium to low plasticity silty sand (ML) according to USCS. Activity of the soil comes from the chloritic-smectitic clay fraction [3]. The activity, $I_A$, is higher than 1.25 in the upper part of the soil profile and decreases from $I_A = 1.25$ to $I_A = 0.75$ below 1 m depth. The clay fraction increases

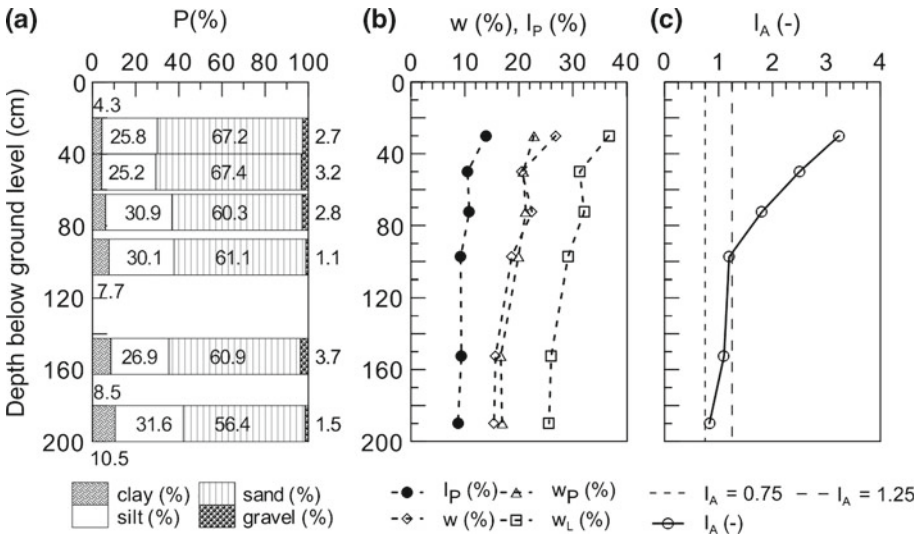


**Fig. 3** **a** Grain size distribution with depth (TP 1); **b** natural water content, Atterberg limits, plasticity index; **c** activity with depth

**Table 1** Mean physical properties of the soil (TP 1), shown in Fig. 4

| w (%) | $I_P$(%) | $\gamma_s$(kN/m$^3$) | $\gamma$(kN/m$^3$) | e (−) | $S_r$(%) |
|---|---|---|---|---|---|
| 19.6 | 9.9 | 25.8 | 16.7 | 0.85 | 60.6 |

with depth from 4% at shallow depths to 10% at about 2 m. The silt fraction also increases with depth from 25 to 32%, while the sand fraction decreases from 67 to 56% (Fig. 3). The increase of the fine fraction with depth may be due to internal erosion from sedimentological and morphological reasons, and downward transport promoted by infiltrating water, flushing the fines into the larger voids surrounding the peds.

As the relevant properties of the soil are mostly influenced by the fines content, undisturbed samples from different depths, with various fines content, were tested in the laboratory experimental programme presented in the following. The location of the test pits from which the samples were retreived is reported in Fig. 4.

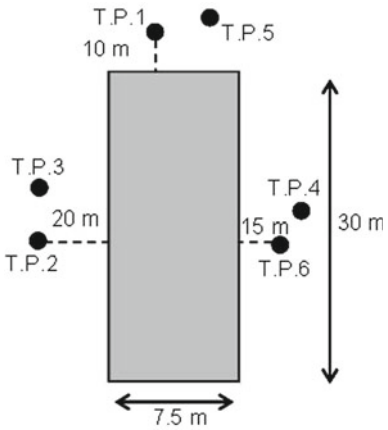


**Fig. 4** Test pit locations, with slope from *top* of the figure to the *bottom*

## 4 Representation of stress paths

The main focus of the experimental programme was to investigate the conditions leading to failure of the silty sand from the 38°–40° steep forest slope in Ruedlingen. To this aim, conventional stress paths, as well as stress paths approaching those experienced in the field were performed.

A preliminary visual inspection of the slope outcrop suggested that any surficial failure would possibly start from the top of the slope, where small, steep, unvegetated scarps were evident. Principal stresses in the field will be inclined to the vertical [4], with the vertical stress exceeding the horizontal stress. The tests in which anisotropic compression was performed before shearing intend to replicate the in situ initial anisotropic stress state, although under axi-symmetric constraint.

In the field the soil is unsaturated, with suction providing a contribution to effective confinement. Extreme rainstorms lead to infiltration and decrease in suction as the soil saturates, until full saturation is achieved when positive pore pressure starts to develop. In consequence, failure is approached along a stress path with reducing confining stress, without a significant change in the shear stress acting. Failure may occur when the soil is still exhibiting unsaturated conditions. Nonetheless, saturated conditions must be analysed first, to provide a convenient reference frame for the behaviour of the soil in an unsaturated condition. In fact, the latter case can be tackled conceptually by considering the behaviour of the reference

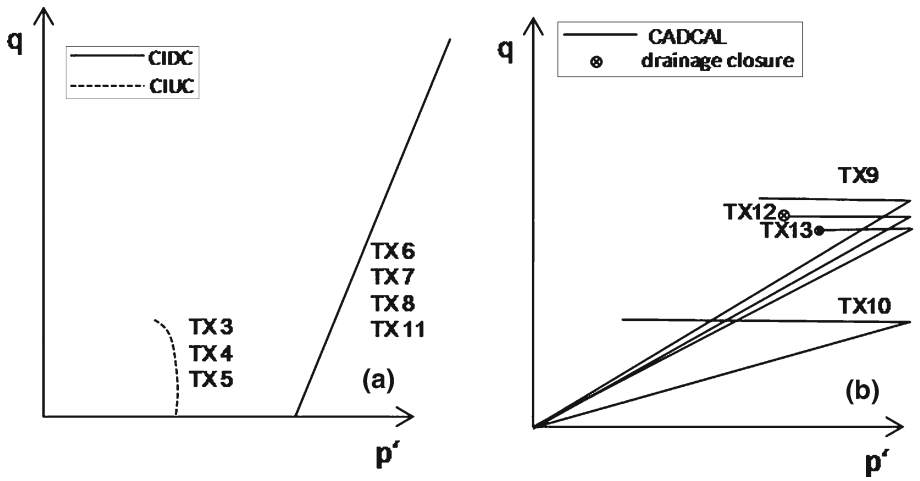


**Fig. 5** Schematic diagram of the stress paths performed: **a** CIDC and CIUC; **b** CADCAL and CADCAL/U

saturated soil subjected to the stabilising effect of suction (e.g. [5–7]).

The following four different stress paths are likely to be relevant in the study of the response of the soil in the slope, namely:

(1) CIDC: isotropic consolidation—standard drained compression (Fig. 5a);
(2) CIUC: isotropic consolidation—standard undrained compression (Fig. 5a);
(3) CADCAL: anisotropic consolidation—drained shear by decreasing mean effective pressure at constant axial load (Fig. 5b);
(4) CADCAL/U: anisotropic consolidation—drained shear by decreasing mean effective pressure at constant axial load, followed by prevention of further drainage to reproduce net undrained conditions (Fig. 5b).

## 5 Testing programme

Conventional drained and undrained compression triaxial tests were performed to study the volumetric behaviour of the soil, and to detect critical state conditions as well as peak shear strength as a function of confining pressure.

Drained shear under constant axial load and increasing water pressure after anisotropic compression (CADCAL) was performed to simulate the stress path experienced in the field by the soil undergoing an infiltration process under its own weight. This kind of stress path is typically suggested to analyse the effect of principal stress ratio increase, eventually leading to failure of soil following water pressure increase in the field [8]. The latter choice is rather common in the context of slope stability (see, e.g., [9]), together with the so called constant shear drained (CSD) stress path, performed by lowering the vertical and the lateral stress (e.g.[8,10,11]). The two stress paths are thought to replicate the range of lateral constraints to the actual stress path in the field. As the onset of failure and attainment of ultimate conditions depend on the stress path followed, together with previous stress history, imposing an initial stress state simulating the anisotropic stress state in the field seems to be more appropriate.

In the last type of stress path (CADCAL/U), a drained shear stage was performed at constant axial load up to a stress ratio slightly lower than the critical stress ratio. Afterwards, the drainage taps in the base and the top pedestals were closed. Pore water pressure and vertical displacement evolution were recorded to investigate better the role of drainage conditions on the mechanical response.

## 6 Failure initiation

Traditionally, peak strength, defined in terms of Mohr–Coulomb's criterion, has been considered as the ruling parameter in the first activation of a slope collapse mechanisms. Although peak strength draws the instantaneous limit locus for admissible stress states, it is well known that unlimited strains may occur even starting from stress states within the limit locus, depending on loading conditions and boundary constraints, as a result of an unstable mechanical response [12]. The occurrence of instability depends on the entire stress and strain history, and it may or may not be promoted as a function of stress increment direction together with the current kinematic constraints (see e.g. [13,14]).

Among unstable responses, static liquefaction is often claimed as the triggering factor in failure of loose granular soil slopes [15–19]. This type of instability has also been referred to as pre-failure instability [16,20,21].

Past researchers have studied the pre-failure instability of sands (see, e.g., [22–28]). The works of Lade and Yamamuro [29,30], Zlatovic and Ishihara [31], Chu et al. [32] and

Wood et al. [33], among others, point out the role played by the grain size distribution on the occurrence of instability.

Nonetheless, different triggering mechanisms may be invoked as a result of some experimental evidence. For example, Take et al. [18] investigated collapse of loose decomposed granite fill slopes subjected to extreme rainfall in centrifuge models, and could not observe flow failure through static liquefaction. They concluded that failure could be more easily triggered by localised transient pore water pressure increase due to soil layering.

From the theoretical point of view, conditions for the possible occurrence of instability have been widely investigated in different contexts starting from ideas presented by Lyapunov [35] and Hill [36]. Following Lyapunov's [35] definition of stability, a stress state for a given strain history is considered stable when a small admissible stress perturbation leads to a small change of the response in strain. In this sense, instability has been identified with large strains promoted by small effective stress perturbations (see, e.g., [16,37] for applications to slope stability). Hill [36] gave a sufficient condition for stability, based on the sign of the second order work. The latter approach has been widely adopted recently both in the analysis of the incremental response of soil elements (see, e.g. [38]) and in the context of slope stability (e.g., [39,40]). The role of time dependency of the mechanical behaviour, that would discriminate between unstable, temporary unstable and stable responses of frictional materials, has been discussed by di Prisco et al. [34].

Deeper understanding of the nature of the strain response of the soil investigated was pursued by applying both criteria to discriminate between stable, temporary unstable and stable stress–strain paths. Two complementary quantities were calculated to examine these possibilities. On the one hand, the second order work, defined as $d^2W = dp'd\varepsilon_v + dqd\varepsilon_q$, with reference to axisymmetric states, was calculated along the experimental stress paths, following Hill's approach [36], in which achieving a positive value is a sufficient condition for the stress path to be stable. Following this criterion, instability may arise whenever the second order work becomes negative.

On the other hand, an unstable mechanism must be characterised by strain acceleration at constant rate boundary loading according to Lyapunov's [35] criterion, with strain acceleration defined as $\ddot{\varepsilon}_i = \frac{\partial^2 \varepsilon_i}{\partial t^2}$, where $\varepsilon_i$ may indicate either a strain component (for axisymmetric strain states, axial or radial strain) or a strain invariant (volumetric or shear strain). For a wider discusson of these criteria see, e.g., Nova [38], Imposimato and Nova [13], Darve and Laouafa [39]; Laouafa and Darve [41].

## 7 Experimental data

The tests were carried out using a fully automated triaxial stress path testing system designed and constructed at the Institute for Geotechnical Engineering—ETHZ (e.g. [42]). The nominal dimensions of the specimens were 50 mm in diameter and 100 mm in height. The soil samples were retrieved from the Ruedlingen site by means of a cylindrical sampler of 100 mm in diameter and 140 mm in height. After extrusion, trimming and mounting in the triaxial cell, the specimens were saturated under back pressure, and the degree of saturation was controlled by performing a B-test after each saturation step. The vertical displacement was measured during saturation, together with water inflow, to infer possible changes of void ratio.

Isotropic and anisotropic drained compression tests to different stress ratios were performed (see Table 2). After volumetric compression, failure was approached following a range of suitable stress paths under different drainage conditions. The standard undrained compression tests, CIUC, were performed starting from initial consolidation pressures ranging from 26 to 76 kPa (see Table 2). These low values

**Table 2** List of the triaxial stress path tests conducted

| Test | $e_0(-)$ | $w_0$ (%) | $\eta(-)$ | $p'_c$(kPa) | Stress path | Depth/test pit |
|---|---|---|---|---|---|---|
| TX3 | 0.816 | 16.0 | 0.00 | 48 | CIUC | 65/80cmTP3 |
| TX4 | 0.790 | 20.0 | 0.00 | 26 | CIUC | 30/50cmTP3 |
| TX5 | 0.950 | 17.5 | 0.00 | 76 | CIUC | 50/65cmTP5 |
| TX6 | 0.811 | 18.0 | 0.00 | 102 | CIDC | 80/95cmTP5 |
| TX7 | 0.783 | 15.0 | 0.00 | 92 | CIDC | 30/50cmTP6 |
| TX8 | 0.899 | 17.4 | Variable | 94 | CIDC | 30/50cmTP6 |
| TX9 | 0.899 | 17.4 | 0.95 | 98 | CADCAL | 40/60cmTP6 |
| TX10 | 0.903 | 15.7 | 0.44 | 99 | CADCAL | 30/50cmTP6 |
| TX11 | 0.890 | 15.3 | 0.00 | 49 | CIDC | 110/125cmTP6 |
| TX12 | 0.928 | 12.0 | 0.90 | 103/69.2 | CADCAL/U | 110/125cmTP6 |
| TX13 | 0.977 | 20.0 | 0.83 | 98/78.6 | CADCAL/U | 40/55cmTP5 |

of consolidation pressure were chosen to simulate appropriate loading conditions of the slope. The tests were intended to provide first information on the potential for unstable response and static liquefaction.

Shearing was performed in the CADCAL tests under constant axial load, by decreasing mean effective stress through increasing pore water pressure, following anisotropic compression. Drained conditions were maintained up to failure in the two CADCAL tests, pore water pressure was increased at a rate of 1 kPa/h for all drained stages, with the top and bottom drainage lines connected to a pore pressure controller, whereas the applied vertical load and radial stress were held constant throughout the tests. In two further CADCAL/U tests, the drainage lines were closed at two different stress ratios (corresponding to the mean effective stress reported in Table 2), slightly below the critical stress ratio, to analyse the effect of hydraulic boundary conditions on the soil response.

The complete testing programme is summarised in Table 2, defining $e_0$ as the initial in situ void ratio, $w_0$ the in situ gravimetric water content, $\eta$ the stress ratio $q/p'$ followed during the consolidation stage. The maximum mean effective stress reached at the end of the consolidation stage is indicated by $p'_c$.

The data collected are reported in terms of:

$$p = \frac{1}{3}(\sigma_a + 2\sigma_r);\ p' = p - u; \quad q = \sigma_a - \sigma_r;$$

$$\varepsilon_q = \frac{2}{3}(\varepsilon_a - \varepsilon_r); \quad \varepsilon_v = \varepsilon_a + 2\varepsilon_r, \quad \Delta u = u - u_0,$$

where $\sigma_a$ is the axial total stress and $\sigma_r$ is the radial total stress applied in the triaxial cell under axisymmetric conditions. Pore water pressure u is measured in both the upper and lower platens, $u_0$ is the reference pore water pressure. Axial strain $\varepsilon_a = -\Delta h/h_0$ where $\Delta h$ was measured over the entire specimen length and $h_0$ is the initial sample height prior to shearing. Volumetric strain $\varepsilon_v = -\Delta V/V_0$ was deduced from water exchange into or out of the specimen, where $\Delta V$ is the change in volume and $V_0$ is the corresponding initial volume prior to shearing. Conventionally, radial strain was derived as $\varepsilon_r = (\varepsilon_v - \varepsilon_a)/2$. Deviatoric stress is defined as $q = \sigma_a - \sigma_r = F/A$, where F is the axial load and A is the current cross sectional area of the specimen, corrected assuming the specimen remained as a right cylinder [43].

The soil shows a fully ductile response in most of the drained tests throughout the whole strain range, as befits the loose packing (Fig. 6a). A smooth peak value of q at $\varepsilon_q \cong 15\%$, was observed in test TX7. Significant compressive

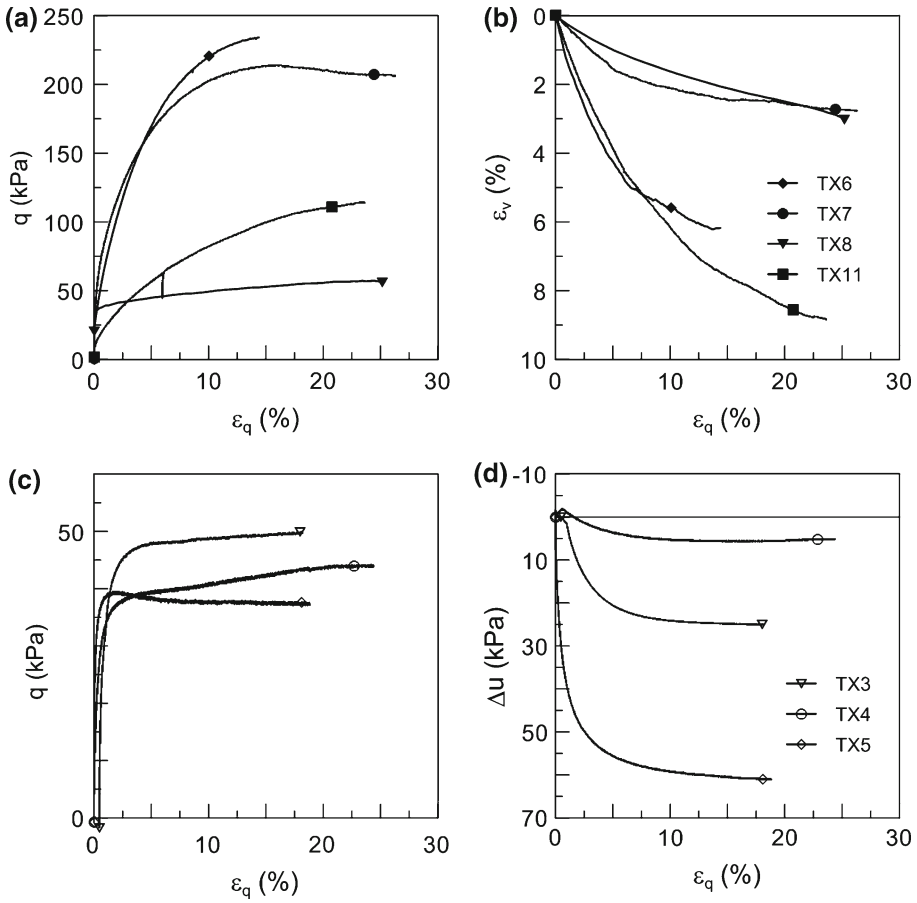


**Fig. 6** Tests results for TX6,7,8,11 in (**a**) and (**b**), for TX3, 4, 5: in (**c**) and (**d**): **a** CIDC; $\varepsilon_q - q$ **b** CIDC $\varepsilon_q - \varepsilon_v$ plane; **c** CIUC; $\varepsilon_q - q$, **d** CIUC $\varepsilon_q - \Delta u$

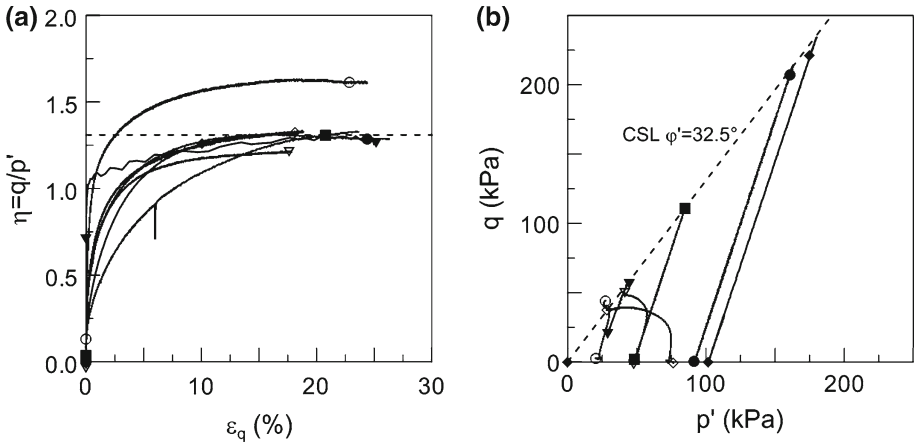


**Fig. 7** CIDC and CIUC results with the same symbols for the 7 triaxial tests as presented in figure 6: **a** $\varepsilon_q - \eta$ plane; **b** $p' - q$ plane

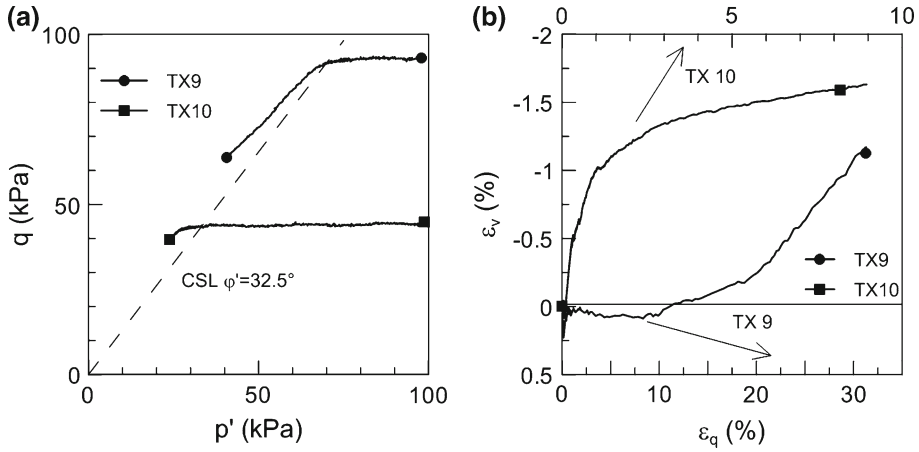


**Fig. 8** CADCAL results: **a** $p' - q$ plane; **c** $\varepsilon_q - \varepsilon_v$ plane, with strain axes at the *top* for TX10 and *bottom* for TX9

volumetric strains $\varepsilon_v$ were recorded in all the drained tests (Fig. 6b), indicating the typical behaviour features of loose soils. In the undrained tests, an increase in pore water pressure is eventually observed (Fig. 6d). The final excess pore water pressure increases with initial confining stress, as expected. A peak in q was observed before ultimate failure in test TX5 (Fig. 6c), followed by a slight decrease of deviator stress at increasing stress ratio.

The results for CIDC and CIUC tests, plotted all together in the $\varepsilon_q - \eta$ plane (Fig. 7a), were exploited to detect a possible critical state stress ratio. In spite of the data variability, typical of natural samples, a value of $\eta_{CS} = 1.30$, corresponding to a critical state friction angle of about $\phi'_{CS} = 32.5°$, seems to represent the critical state conditions for this soil fairly well. The only exception is noted in test TX4 (Fig. 7a), which was carried out at the lowest confining pressure (Fig. 7b) and therefore this is to be expected. The entire set of stress paths followed by the soil in the standard tests is summarised in Fig. 7b, where the assumed critical state line (CSL) is drawn.

### 7.1 CADCAL and CADCAL/U results

The results of the CADCAL results are reported in the planes $p' - q$ (Fig. 8a) and $\varepsilon_q - \varepsilon_v$ (Fig. 8b). Specimens TX9 and TX10 were compressed anisotropically up to $p' \approx 100$ kPa with $\eta = 0.95$ and $\eta = 0.44$, respectively. Increasing the pore water pressure promotes a slight increase in volumetric strain (Fig. 8b), which is likely to be the result of elastic swelling as the stress path moves inside the yield locus. For the sample TX10, which was previously compressed at the low stress ratio of $\eta = 0.44$, a definite increase in shear strain was observed just after the critical state stress ratio, characterised by an increase in volumetric strain. The latter denotes a dilatant mode of ultimate failure with plastic volume increase. The sample TX9, which was compressed at a higher stress ratio of $\eta = 0.95$, eventually reached a dilatant mode of failure, but after a first contractant stage until a deviatoric strain of 10%. In both tests, the ultimate failure stress ratio lies above the cristical state line, reaching values of $\eta = 1.4$ at least.

Specimens TX12 and TX13 were compressed anisotropically up to $p' \approx 100$ kPa with $\eta = 0.90$ and $\eta = 0.83$, respectively. The pore water pressure was increased, causing p' to reduce up to a stress ratio $\eta$ of slightly less than 1.3 and 1.1, respectively, (Fig. 9a), hence below the critical state stress ratio.

An increase in pore water pressure at constant deviator stress was the first evidence of the sample response (Fig. 9b), with the first small instantaneous peak of water pressure

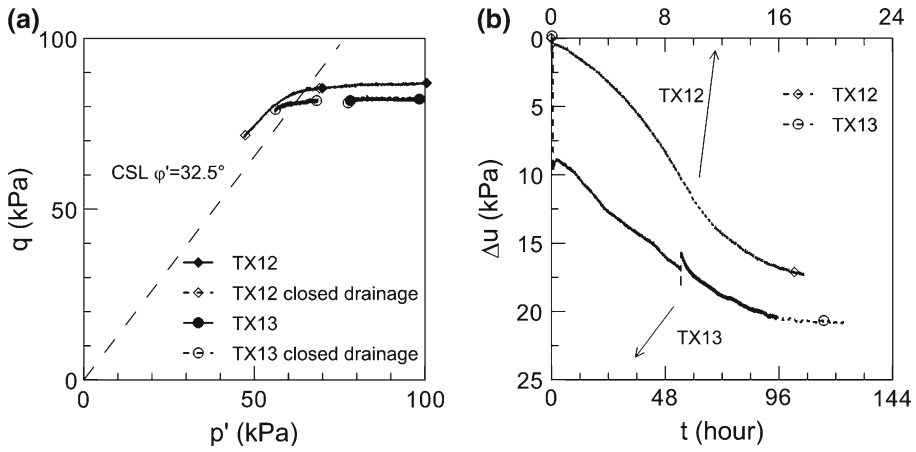


**Fig. 9** CADCAL/U results: **a** $p' - q$ plane; **b** $t - \Delta u$ plane

presumed to be due to closing the drainage lines. Nonetheless, even after the initial pore pressure step, the stress state is still below the critical state line, but the pore pressure continues to increase without further change of external loading conditions. The rate of pore pressure increase depended on the distance of the stress ratio from the critical state line at the time of drainage closure, as highlighted by Fig. 9b. The stress path passes over the critical state line, eventually leading to failure for a stress ratio comparable to the one reached in drained conditions.

## 8 Discussion and interpretation of the results

Data of the compression stage for samples collected from z = 0.0 m to z = 0.5 m are reported in Fig. 10a, while Fig. 10b depicts the same data for the samples collected at greater depths. The two data sets were separated to evaluate the influence of fines content on the soil volumetric behaviour.

The first data set (Fig. 10a) suggests typical features of loose granular soils; compressibility tends to increase with stress ratio, due to fabric anisotropy, though the different compression curves do not converge towards a unique normal compression line in the stress range investigated. The compressibility coefficients are rather high in any case, ranging from $C_c = 0.14$ in the isotropic compression path to $C_c = 0.21$ for the test performed at a stress ratio of $\eta = 0.83$. This shows that the fines content influences the compressibility of the soil. The behaviour of the samples collected at greater depths (Fig. 10b) seem to show more of the characteristic features of fine grained soils. The curves tend to converge more rapidly to a unique normal compression line, in the stress range investigated. The compressibility coefficients lie in the range from $C_c = 0.20 \div 0.26$. Previous oedometer tests, performed over a wider stress range, had given a compressibility coefficient $C_c = 0.25$ [2], suggesting a reference natural logarithmic equivalent $\lambda = 0.11$.

A tentative critical state line is drawn in the $e - \ln(p'/p'_{ref})$ plane in Fig. 11 ($p'_{ref} = 1$.kPa). Void ratios for $\eta = 1.3$ are reported for all of the triaxial tests, and these points correspond mainly to asymptotic values of volumetric strain in drained tests or of pore pressure in undrained tests (see Fig. 6). Data of samples collected at depths $z \geq 0.5$ m (filled symbols) seem to represent a unique critical state line, again with an inclination of $\lambda = 0.11$. Data from samples collected at lower depths (open symbols) present much higher scatter, although convergence to the previous critical state line is observed for the higher stresses investigated. All together, the results suggest that this soil shares typical features of the so called "transitional soils", typically including mainly silts with different percentages of clay and sand (see, e.g., [44]).

Peak stress ratios reached in all the tests in which the critical state angle was exceeded, are presented in Fig. 12, as a function of the mean effective stress at failure. Open symbols indicate values for the samples collected at depths $z \geq 0.5$ m, while filled symbols represent values for samples collected at greater depths. As expected, the peak stress ratio decreased with increasing mean effective stress and it was generally greater in the upper soil layer.

The peak stress ratio was reached with a diffuse, rather than a localised, mode of failure in all the tests performed. A similar failure mechanism is expected when an unstable liquefaction response is triggered along the stress path. A diffuse failure mode was observed, for example, by Han and Vardoulakis [45] and Khoa et al. [46] in undrained axial strain controlled compression tests on clean loose sand. Nonetheless, in this case the samples did not collapse with a run-away mode of failure. Significant increase in the cross sectional area during compression under constant axial load caused the applied deviator stress to be reduced progressively and the test control was never lost. The evolution of second order work and of strain acceleration along the stress paths investigated were then systematically exploited, to detect the nature of the strain response of the soil. It is worth noting that the absolute value of the second order work has no intrinsic meaning, depend-

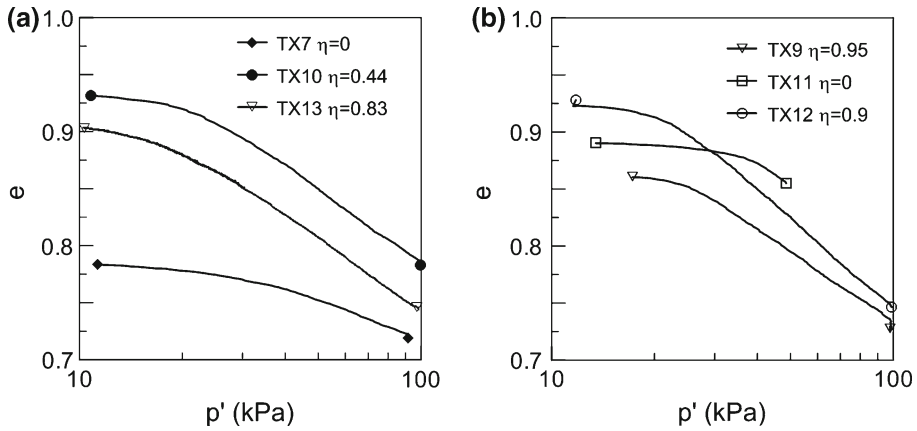


**Fig. 10** Consolidation curves for the two data sets: **a** Set 1—depth z = 0.0 ÷ 0.5 m; **b** Set 2—depth, z > 0.50 m

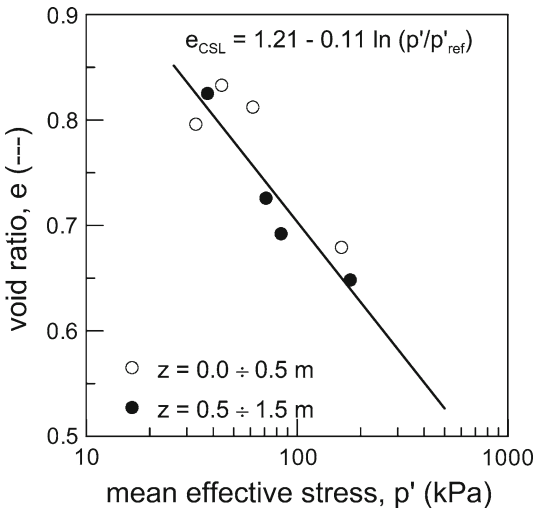


**Fig. 11** Projection of the critical state line in the $e - \ln(p'/p'_{ref})$ plane

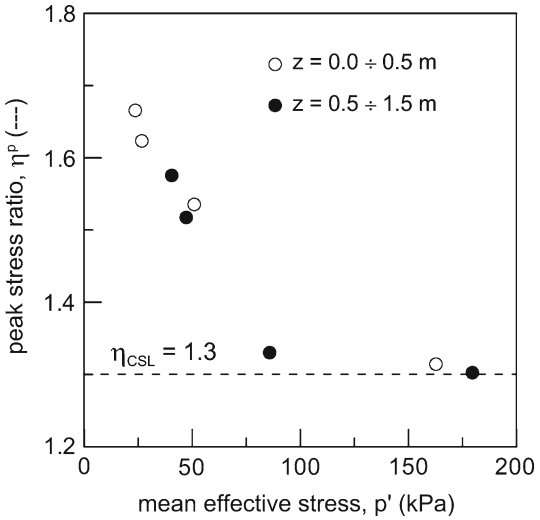


**Fig. 12** Peak stress ratios as a function of mean effective stress at failure

ing on the strain interval adopted in the data elaboration. In the following discussion, only its sign will be of relevance.

Results for specimen TX5 are presented first in Fig. 13. The classical potential instability line, defined as the stress ratio at which the peak deviator stress occurs, MIL = 1.0, is depicted in the $p' - q$ plane in Fig. 13a. The data are compared with the value of the second order work along the undrained path in Fig. 13b, which clearly shows that a null value is approached for the same stress ratio. It is worth noting that in this case, hence along a conventional undrained triaxial compression, the second order work remained around zero throughout the rest of the test, denoting a conditionally stable response rather than a proper unstable response. No strain acceleration was observed until the end of the test.

Results of the two tests TX10 and TX9 are presented in Figs. 14 and 15, which are considered to be more representative of the stress history leading to local failure of the soil in the slope. The data refer to the stage in which, after anisotropic consolidation, the samples were sheared under constant axial load by decreasing mean effective stress under drained conditions.

The results for sample TX10, are summarised in Fig. 14. Figure 14a reports the incremental plastic work, defined as $dW^p = dp'(d\varepsilon_v - d\varepsilon_v^e) + dq(d\varepsilon_q - d\varepsilon_q^e)$, where the elastic strain increments were calculated assuming a slope of the unloading-reloading line $\kappa = 0.007$ [2] and a constant Poisson's ratio $\upsilon = 0.3$. The trend shows that the stress ratio $\eta$ exceeds that of the critical state line because the stress path is still inside the elastic locus. Incremental plastic work begins to increase at about $\eta = 1.45$, where the stress state reaches the yield surface. Although in a dilatant regime (Fig. 8b), the stress ratio could still increase further. Second order work remains mainly positive (Fig. 14b), denoting a stable hardening response of the soil, until a value of $\eta = 1.5$ is reached, where the sign of the second order work changes, becoming definitely negative. The latter stress ratio seems to define the onset of failure in this test. The result is confirmed by the evolution of the shear strain acceleration, which clearly

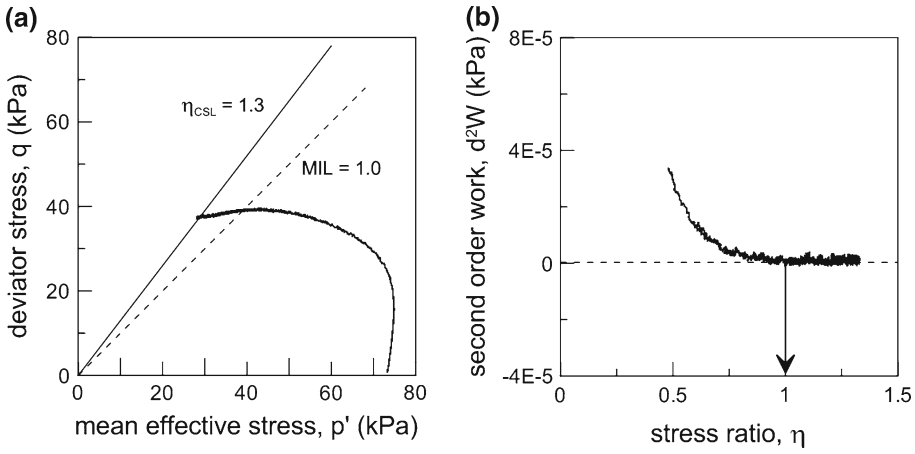


**Fig. 13** Test TX5: **a** stress path in the p′ − q plane and **b** evolution of second order work with stress ratio

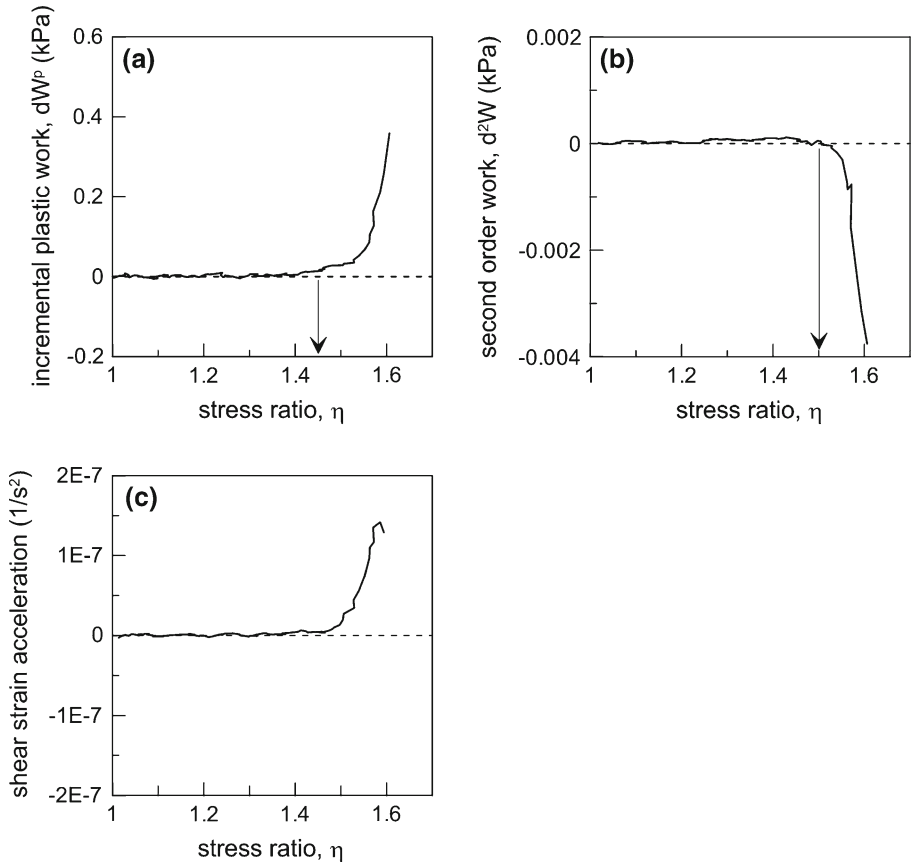


**Fig. 14** Test TX10: **a** incremental plastic work; **b** evolution of second order work; **c** shear strain acceleration

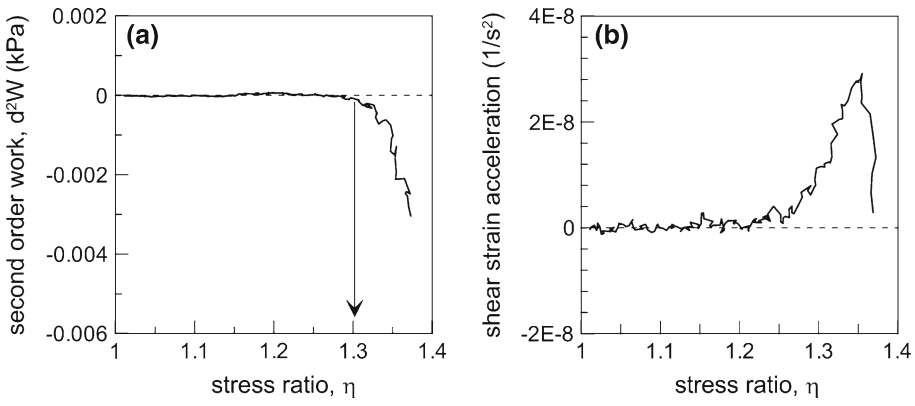


**Fig. 15** Test TX9: **a** shear strain acceleration; **b** evolution of second order work

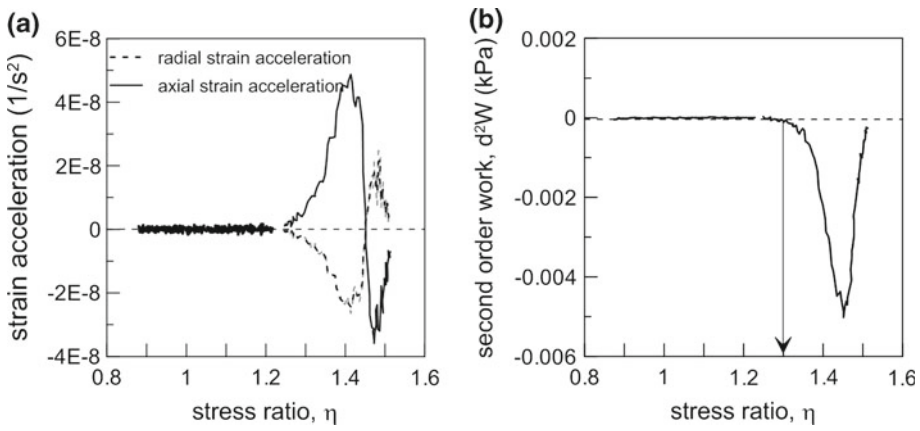


**Fig. 16** Test TX12: **a** radial and axial strain acceleration; **b** evolution of second order work

increases, starting from the same stress ratio. Slightly higher stress ratios, almost compatible with the average slope inclination, which is represented by a stress ratio of $\eta = 1.55$ to 1.63 with reference to axisymmetric conditions, could be achieved eventually in the test, but only as a result of the substantial increase of the specimen's cross sectional area under constant axial load, promoted by diffuse failure.

Similar qualitative behaviour could be observed in test TX9 (see Fig. 15), except that, in this case, the onset of instability was observed for $\eta \approx 1.3$, hence for a stress ratio nearly equal to the critical state line. Nonetheless, the following trend is analogous to the previous one. Slightly higher stress ratios were reached, already after the onset of diffuse failure, at increasing shear strain acceleration until the peak, where shear strain began to decelerate as a result of the dilatant mode of ultimate failure (Fig. 8b).

The results of the two tests suggest that the behaviour of the undisturbed soil in a shearing path at constant axial load is conditionally stable [16], instability may occur provided that the mean effective stress was reduced continuously.

The drainage lines were closed in the triaxial tests TX12 and TX13 at stress ratios lower than those corresponding to critical state, after a preliminary drained shear stage, to verify the effect of drainage constraint on the behaviour of the soil. In both tests, positive increase in pore water pressure was recorded throughout the whole test duration. Failure was reached in the two tests at stress ratios comparable to those attained in drained conditions, but at a significantly lower strain rate. Axial and radial strain accelerations are reported in Fig. 16a during the undrained stage of test TX12. The figure shows that upon drainage closure, strains started to increase at an accelerating rate comparable to that observed in the drained CADCAL tests. Second order work (Fig. 16b) becomes negative for a stress ratio of about 1.3, decreases temporarily and reaches a minimum, after which it increases again tending to null values. The magnitude of strain acceleration also decreases after reaching a maximum value, and the two components (axial and radial) are reversed at a certain point, denoting a change in the deformational response of the soil, and they both tend to small values upon reaching the peak stress ratio at decreasing deviator stress.

The results for test TX13 are reported in Fig. 17. At the scale of the other tests (Fig. 17a–b) the data are close to zero throughout the whole test duration. Nonetheless, a magnified scale (Fig. 17c–d) reveals that the pattern of behaviour is the same as the previous test, although at a much lower strain rate. Both strain acceleration and second order work values are much smaller than those in test TX12 by at least two orders of magnitude, and failure is attained at a very slow rate, with pore pressure rate eventually decreasing, as already pointed out in the presentation of the experimental data (ref. Fig. 9). Nonetheless, a diffuse mode also characterised the failure this specimen, although the drainage line was closed well below the critical state line. The trend of both strain acceleration and second order work denote a temporarily unstable response, starting from the stress ratio for which the second order work may be assumed to be negative, $\eta = 1.28$.

As already pointed out by di Prisco et al. [34], temporarily unstable response may be explained if time dependent stress–strain behaviour is taken into account. Adopting a visco-plastic model for the behaviour of sands, the authors showed that temporary unstable response, characterised by increasing and then decreasing strain rate, could be interpreted as the result of two competing rate dependent, hardening and softening respectively, mechanisms.

The experimental results presented here seem to suggest similar conclusions. In fact, although ultimate failure is dilatant, secondary compressive strains may play a significant role, promoting pore pressure increase under undrained conditions. Secondary compressibility may come from the clear bi-modal pore size density function characterising this soil [3], promoting an internal re-distribution of pore water pressure [47], or simply from the effect of organic matter and of the activity of the fine fraction of the soil. In both cases, the development of strains during pore pressure increase along the undrained stress paths at constant axial load seems to be affected clearly by the resulting time dependent response.

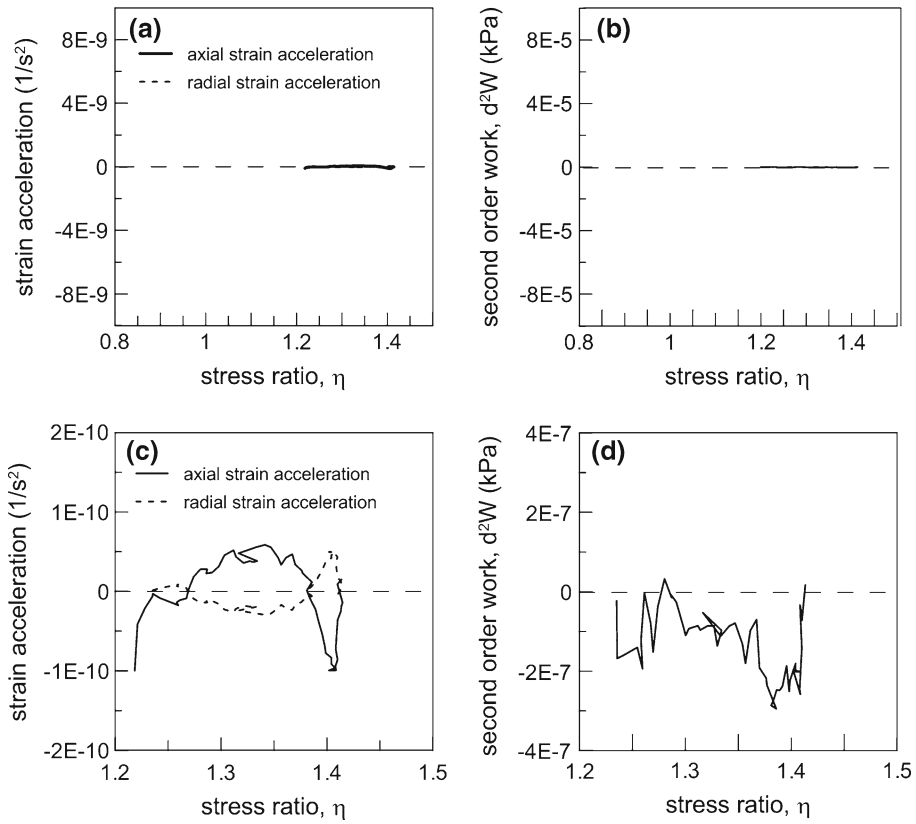


**Fig. 17** Test TX13: **a** radial and axial strain acceleration; **b** evolution of second order work **c** magnified accelerations; **d** magnified second order work

To provide a synthetic criterion for the onset of failure on the basis of the results collected, the framework proposed by Chu et al. [16] was exploited. Starting from the proposal of Been and Jefferies [48], the authors proposed a modified state parameter to normalise the stress ratio corresponding to the onset of instability ($M_{IL}$). The modified state parameter, $e_{IL} - e_{cr}$, is defined as the difference between the void ratio at the onset of instability, $e_{IL}$, and the void ratio, $e_{cr}$, at the critical state at the same effective mean stress. They succeeded in distinguishing the occurrence of conditional stability from that of run-away failure, based on both the state parameter and the drainage conditions. They concluded that instability can be triggered for positive values of $e_{IL} - e_{cr}$ at stress ratios lower than the critical state both in drained and undrained conditions. In the first case conditional (temporary) instability can be promoted at continuously decreasing mean effective stress. In undrained conditions, run-away failure is expected due to progressive pore pressure increase. For negative values of $e_{IL} - e_{cr}$ only conditional instability may be experienced by the soil, and only if drained conditions were maintained while decreasing mean effective stress.

The modified state parameter calculated for tests TX9, TX10 and TX5, and shown in Fig. 18, seems to fit quite well in the Chu et al. [16] framework, suggesting that the onset of failure may be possibly described by a measure of the current void ratio with respect to critical state. Nonetheless,

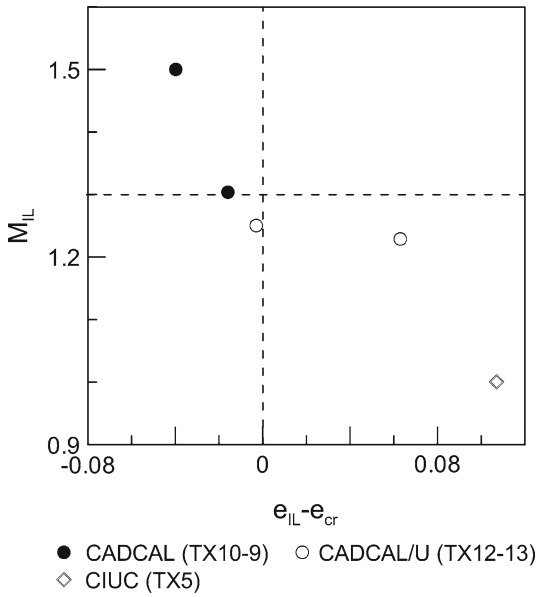


**Fig. 18** Results for the inclination of the potential instability line, MIL, as a function of Been and Jefferies parameter modified by Chu et al. [16]

no run-away failure was ever detected for the soil investigated, but conditional stability was always promoted along all type of stress paths investigated, possibly due to both the

stabilising effect of fines content on the sand grain skeleton and the specific boundary constraints in the tests.

Two more points are drawn with open round symbols in the figure for tests TX12 and TX13, corresponding to the void ratios at the time when the drainage lines were closed, and failure began to be triggered, albeit slowly. Although also these points fit the trend of a decreasing MIL inclination with increasing $e_{IL} - e_{cr}$, it's worth pointing out that only time dependent stress–strain behaviour, and not only void ratio alone, may justify the occurrence of failure in these tests.

## 9 Concluding remarks

The response of the undisturbed samples suggests that the soil investigated may be typically classified into the so-called transitional soil, which shares some typical features of loose granular soils, such as strain induced anisotropy and potential for instability along standard undrained compression. The fines content plays a definite role in the behaviour, both conferring time dependent high compressibility, in the range for fine grained soils, and providing a stabilising effect on the potential unstable mechanisms.

The peak stress ratios that the soil could reach in saturated conditions were rather high, along the paths simulating decrease of effective pressure promoted by rainfall infiltration, especially at the low confining pressures expected for surficial soil elements, and they were almost compatible with the average slope inclination. Nonetheless, these high stress ratios could be reached in the tests only thanks to an increase in the cross-sectional area of the specimens after the onset of failure, which can be described better by the inclination of the potential instability line $M_{IL}$. The behaviour of the soil was not properly unstable in the stress paths analysed, but temporary instability, denoted by strain acceleration at constant external loading rate, triggered the soil failure in any case. Time dependent compressibility plays a significant role, as the onset of failure could be triggered by closing the drainage tap, after an increase in pore water pressure, even starting from stress states below the critical state line. Hence, the occurrence of failure appears to be a function of time dependent compressibility, as well as the distance from the critical state line measured in terms of void ratio.

The experimental investigation suggests that a constitutive model allowing for the description of the transitional characteristics of the soil behaviour should be adopted in the analysis of the slope. Unsaturated conditions may be accommodated, starting from a suitable reference model conceived for saturated conditions (e.g. [49]). Typical volumetric behaviour of fine grained soils, strain induced anisotropy, and possibly time dependence, are basic requirements in the choice of a reference model for saturated conditions. An experimental programme, extending the study of the stress–strain behaviour of the soil to unsaturated conditions, is in progress.

**Acknowledgments** This research was funded by the Competence Centre for Environment and Sustainability (CCES) within the framework of the TRAMM—Project. The authors are grateful to Amin Askarinejad, Lorenzo Colombo, Peter Kienzler, Marco Sperl, Ernst Bleiker and Rico Borrellini, who either carried out the fieldwork or helped with the laboratory apparatus. We are also most grateful to the Gemeinde Ruedlingen and their President Katy Leutenegger for giving permission to carry out this experiment on their land. The contribution of the two anonymous reviewers, who helped significantly in improving the quality of the paper, is also gratefully acknowledged.

## References

1. Fischer, C., López, J., Springman, S.M.: Remediation of an eroded steep slope in weathered sandstone after a major rainstorm. In: International Conference on Landslides, pp. 878–883. Hong Kong (2003)
2. Springman, S.M., Kienzler, P., Casini, F., Askarinejad, A.: Landslide triggering experiment in a steep forested slope in Switzerland. In: 17th International Conference on Soil Mechanics and Geotechnical Engineering, 5–9 Oct, Alexandria (2009)
3. Colombo, L.: Large shear box for analysing strength mobilisation in unsaturated conditions. Master Thesis, Politecnico di Milano (2009)
4. Vaughan, P.R., Kwan, C.W.: Weathering, structure and in situ stress residual soils. Géotechnique **34**(1), 43–59 (1984)
5. Jommi, C.: Remarks on the constitutive modeling of unsaturated soils. Exp. Evid. And Theor. Approaches in Unsaturated Soils, Tarantino, Mancuso Eds., Balkema, Rotterdam, pp. 139–153 (2000)
6. Vaunat, J., Gens, A., Pontes Filho I.D.S.: Application of localization concepts to discontinuous water content patterns in unsaturated media. In: Proceedings of NUMOG VIII, vol. 1, pp. 179–184. Swets and Zeitlinger, Lisse (2002)
7. Buscarnera, G., Nova, R.: Modelling instabilities in triaxial testing on unsaturated soil specimens. Int. J. Numer. Anal. Meth. Geomech. (2009). doi:10.102/nag.832
8. Anderson, S.A., Sitar, N.: Analysis of rainfall-induced debris flows. J. Geotech. Eng. ASCE **121**, 544–552 (1995)
9. Ng, C.W.W., Fung, W.T., Cheul, C.Y., Zhang, L.: Influence of stress ratio and stress path on behavior of loose decomposed granite. J. Geotech. Eng. ASCE **130**(1), 36–44 (2004)
10. Anderson, S.A., Riemer, M.F.: Collapse of saturated soil due to reduction in confinement. J. Geotech. Eng. ASCE **121**, 216–220 (1995)
11. Springman, S.M., Jommi, C., Teysseire, P.: Instability on moraine slopes induced by loss suction: a case history. Géotechnique **53**(1), 3–10 (2003)
12. Nova, R.: The failure concept in soil mechanics revisited. In: Labuz, J.F., Drescher, A. (eds.) Bifurcations and Instabilities of Geomechanics, pp. 3–16. Balkema, Lisse (2003)
13. Imposimato, S., Nova, R.: An investigation on existence and uniqueness of the incremental response of elastoplastic models for virgin sand. Mech. Cohes.-Frict. Mater. **3**, 1–16 (1998)
14. Lancelot, L., Shahrour, I., Mahmoud, A.M.: Instability and static liquefaction on proportional strain paths for sand at low stresses. J. Eng. Mech. ASCE **130**(11), 1365–1372 (2004)
15. Wang, G., Sassa, K.: Factors affecting rainfall-induced landslides in laboratory flume tests. Géotechnique **51**(7), 587–599 (2001)

16. Chu, J., Leroueil, S., Leong, W.K.: Unstable behaviour of sand and its implication for slope instability. Can. Geotech. J. **40**, 873–885 (2003)
17. Olivares, L., Picarelli, L.: Shallow landslides triggered by intense rainfalls on natural slopes covered by loose unsaturated pyroclastic soils. Géotechnique **53**(2), 283–287 (2003)
18. Take, W.A., Bolton, M.D., Wong, P.C.P., Yeung, F.J.: Evaluation of landslide triggering mechanisms in model fill slopes. Landslides **1**, 173–184 (2004)
19. Ng, C.W.W., Springman, S.M., Alonso, E.E.: Monitoring the performance of unsaturated soil slopes. J. Geotech. Geoenviron. Eng. **6**, 799–816 (2008)
20. Lade, P.V.: Experimental observations of stability, instability and shear planes in granular materials. Ing. Arch. **59**(2), 114–123 (1989)
21. Lade, P.V., Pradel, D.: Instabilty and plasti flow of soils. 1: Experimental observations. J. Eng. Mech. ASCE **116**(1), 2532–2550 (1990)
22. Castro, G., Poulos, S.J.: Factors affecting liquefaction and cicling mobility. J. Geotech. Eng. ASCE **103**(6), 501–516 (1977)
23. Vaid, Y.P., Chern, J.C.: Cyclic and monotonic undrained response of saturated sands. Adv. in the Art of Test. Soils Under Cycl. Cond., Am. Soc. of Civ. Eng. Convention, Detroit, pp. 120–1478 (1985)
24. Lade, P.V., Nelson, R.B., Ito, Y.M.: Non-associated flow and stability for granular materials. J. Eng. Mech. ASCE **113**(9), 1302–1318 (1987)
25. Lade, P.V., Nelson, R.B., Ito, Y.M.: Instability of granular materials with non-assoiated flow. J. Eng. Mech. ASCE **114**(2), 2173–2191 (1988)
26. Lade, P.V., Bopp, P.A., Peteres, J.F.: Instability of dilating sand. Mech. Mater. **16**, 249–264 (1993)
27. di Prisco, C., Imposimato, S.: Time dependent mechanical behaviour of loose sand. Mech. Cohes.-Frict. Mater. **17**(1), 45–73 (1996)
28. di Prisco, C., Imposimato, S.: Experimental analysis and theoretical interpretation of triaxial load controlled loose sand collapses. Mech. Cohes.-Frict. Mater. **18**(2), 93–120 (1997)
29. Lade, P.V., Yamamuro, J.A.: Effects of non-plastic fines on static liquefaction of sands. Can. Geotech. J. **34**, 905–917 (1997)
30. Yamamuro, J.A., Lade, P.V.: Steady-state concepts and static liquefaction of silty sands. J. Geotech. Geoenviron. Eng. **9**, 868–877 (1998)
31. Zlatovic, S., Ishihara, K.: Normalized behavior of very loose nonplastic soils: effects of fabric. Soils Found. **37**(4), 47–56 (1997)
32. Chu, J., Leong, W.K.: Effect of fines instability behaviour of looose sand. Géotechnique **52**(10), 751–755 (2002)
33. Wood, F.M., Yamamuro, J.A., Lade, P.V.: Effect of depositional method on the undrained response of silty sand. Can. Geotech. J. **45**, 1525–1537 (2008)
34. di Prisco, C., Imposimato, S., Vardoulakis, I.: Mechanical modelling of drained creep triaxial tests on loose sands. Géotechnique **50**(1), 73–82 (2000)
35. Lyapunov, A.M.: Problème général de la stabilitè des mouvements. Annales de la Faculté de Sciences de Toulouse **9**, 203–274 (1907)
36. Hill, R.: A general theory of uniqueness and stability in elastoplastic solids. J. Mech. Phys. Solids **6**, 236–249 (1958)
37. Vaid, Y.P., Eliadorani, A.: Instability and liquefaction of granular soils under undrained and partially drained states. Can. Geotech. J. **35**, 1053–1062 (1998)
38. Nova, R.: Controllability of the incremental response of soils specimens subjected to arbitrary loading programmes. J. Mech. Behav. Mater. **5**(2), 193–201 (1994)
39. Darve, F., Laouafa, F.: Instabilties in granular materials and application to landslides. Mech. Cohes.-Frict. Mater. **5**, 627–652 (2000)
40. Lignon, S., Laouafa, F., Punier, F., Khoa, H.D.V., Darve, F.: Hydro-mechanical modelling of landslides with a material instability criterion. Géotechnique **59**(6), 513–524 (2009)
41. Laouafa, F., Darve, F.: Modelling of slope failure by a material instability mechanism. Comput. Geotech. **29**, 301–325 (2002)
42. Arenson, L.: Unstable alpine permafrost: a potentially important natural hazard. Ph.D dissertation, IGT_ETHZ, http://e-collection.ethbib.ethz.ch/show?type=diss&nr=14801, Zürich (2002)
43. Head, K.H.: Manual of soil laboratory testing, 3: effective stress tests. Wiley, Chichester (1998)
44. Nocilla, A., Coop, M.R., Colleselli, F.: The mechanics of an Italian silt: an example of 'transitional' behaviour. Géotechnique **56**(4), 261–271 (2006)
45. Han, C., Vardoulakis, I.: Plane-strain compression experiments on water-saturated finr-grained sand. Géotechnique **41**(1), 49–78 (1991)
46. Khoa, H.D.V., Georgopulos, I.O., Darve, F., Laouafa, F.: Diffuse failure in geomaterilas: experiments and modeling. Comput. Geotech. **33**, 1–14 (2006)
47. Navarro, V., Alonso, E.E.: Secondary compression of clays as a local dehydration process. Géotechnique **51**(10), 859–869 (2001)
48. Been, K., Jefferies, M.G.: A state parameter for sands. Géotechnique **35**(2), 99–112 (1985)
49. Romero, E., Jommi, C.: An insight into the role of hydraulic history on the volume changes and anisotropic clavey soils. Water Resources Research, **44**, (2008) doi:10.1029/2007WR006558